42nd AIAA/ASME/SAE/ASEE Joint Propulsion Conference & Exhibit
9 - 12 July 2006, Sacramento, California

AIAA 2006-5044

Multi-Scale Porous Media Modeling for Liquid Rocket Injector Applications

Emre Sozer*, Wei Shyy†
University of Michigan, Ann Arbor, MI, 48109

and

Siddharth Thakur‡
University of Florida, Gainesville, FL, 32611

Porous materials are often used for the injector face plate of liquid propellant rocket engines (LPRE). To develop predictive capabilities for such porous media fuel flow problems, a multi-scale modeling strategy is developed. The effect of porous structure on the macroscopic fluid flow is accounted for via local volume averaged governing equations. The resulting set of transport equations, at the global domain level, contains closure terms representing the statistical flow characteristics around the pores. Conventionally, the closure terms are evaluated using empirical correlations. In the present approach, these closure terms in the global fluid flow equations are deduced via direct computation of the fluid flow in individual, representative pores. Hence, empirical dependence of simulations can be removed without requiring excessive computational cost. The performance of the present approach is demonstrated by studying isothermal fluid flow through a porous plate with an array of uniformly drilled holes. As a preliminary step towards multi-scale closure of the energy equation, a global scale heat transfer analysis case is also conducted to illustrate the scope of the entire theoretical framework.

Nomenclature

A	=	cross-sectional area
A_{sf}	=	solid-fluid interfacial area
C_E	=	Ergun coefficient
C_f	=	skin friction coefficient
c_p	=	specific heat
D_{ij}^d	=	dispersion tensor
Da	=	Darcy number
δ_{ij}	=	Kronecker delta
ε	=	porosity
F_τ	=	net skin friction force
H	=	channel height
K	=	permeability
L	=	channel length
k_f	=	fluid phase thermal conductivity
k_s	=	solid phase thermal conductivity
K_{ij}^e	=	effective thermal conductivity tensor

* Graduate Student, Aerospace Engineering Department
† Clarence L. "Kelly" Johnson Collegiate Professor and Chair, Aerospace Engineering Department
‡ Associate Research Scientist, Mechanical and Aerospace Engineering Department

$\dot{m}$ = mass flow rate
μ = dynamic viscosity
n_i = surface normal vector
p = pressure
p_i = inlet pressure
p_e = exit pressure
ΔP_E = Experimental measurement of pressure drop across the plate
ΔP_C = Computed pressure drop across the plate with K and C_E estimated from pore scale analysis
$\Delta P_{C_E} / \Delta P_K$ = Proportion of pressure drops due to inertial and Darcian terms
ρ = fluid density
Re = Reynolds number
Re_d = Reynolds number based on pore diameter
$\mathrm{Re}_{\sqrt{K}}$ = Reynolds number based on permeability
S_{ij} = strain rate tensor
T_{ij} = stress tensor
T = temperature
θ_w = dimensionless wall temperature
u_D = filter velocity
u_i = velocity vector
U_e = exit velocity
V_f = volume of the fluid phase
V = total volume

I. Introduction

Porous materials are often used for the injector face plate of liquid propellant rocket engines (LPRE). Fuel bleeds through the porous plate to aid in cooling of the injector face by transpiration while helping injection of fuel at the same time. For example, in P&W's RL10 engine and Space Shuttle Main Engine (SSME), Rigimesh™ is used. It is formed by pressing layers of sintered stainless steel wire meshes (see Figure 1). In the case of SSME, a 0.25" thick plate with about 9% void space is used. Rigimesh can qualitatively be classified as a dense, non-uniform, fibrous porous media.

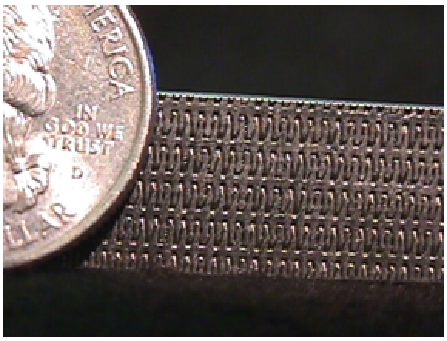

Figure 1. Rigimesh material

In such porous fluid flow problems, direct numerical simulation of the fluid flow accounting for all geometric details is very costly if not impossible. Thus modeling efforts in this area dating back to Darcy's experimental study in 1856, have mostly aimed at correlating the pore level flow effects to the bulk fluid motion. Conventionally, the closure terms have been evaluated using empirical correlations. The most commonly used approach is to add source terms to the global transport equation of mass, momentum and energy. The source terms are largely based on those

proposed by Darcy[1] and Ergun[3], via two parameters, namely, permeability, K, and the Ergun coefficient, C_E. These parameters are generally determined via empirical correlations (See Ref. 11).

To develop predictive capabilities for such porous media flow problems, a first principle-based, multi-scale modeling strategy is developed. The effect of porous media on the macroscopic fluid flow structures is accounted for via local volume averaged governing equations. The resulting set of transport equations, at the global domain level, contains closure terms representing the statistical flow characteristics around the pores. Our approach is based on the local volume averaging method. This method follows the notion of investigating the flow properties averaged over local volume elements and produces an unclosed set of governing equations. Most porous media can be thought of as a matrix of repeating pore patterns. We can calculate the closure terms for different flow speeds and pore patterns observed. These results can be interpolated to obtain the closure term evaluations throughout the porous medium. Thus, we can avoid the computational cost of direct simulation yet we can produce accurate numerical predictions completely free of empiricism. In the present approach, these closure terms in the global fluid flow equations are deduced via direct computation of the fluid flow in individual, representative pores.

In the following sections, we first briefly review the theoretical background followed by detailed derivations of local volume averaged governing equations. We then explain the conventional and multi-scale closure methodologies. Although our ultimate objective in this study is to develop a method to accurately simulate the fluid flow and heat transfer through the Rigimesh™ material, we first examine our methodology for a simpler porous medium with well defined pore geometry. The performance of the present approach is demonstrated by studying isothermal fluid flow through a simple porous medium of a plate with an array of uniform drilled holes and comparing our findings with those of Tully et al.[15] As a preliminary step towards multi-scale closure of the energy equation, a global scale heat transfer analysis case is also conducted to illustrate the scope of the entire theoretical framework.

II. Multi-Scale Porous Media Model

A. Representative Elementary Volume and Porosity

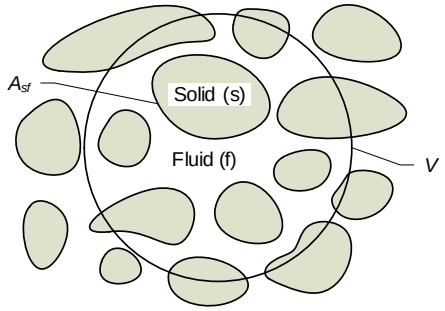

Figure 2. Schematic of a representative elementary volume (REV).

Many porous media flow problems involve a wide range of length scales which are generally too costly to fully resolve. An intuitive approach to this problem is to impose the average effect of the pores on global flow structures. But first a sensible scale for averaging needs to be defined. An averaging volume should be sized small enough in order to not filter global flow structures but it should be large enough so as to guarantee containing both fluid and solid phases at all times. In literature, such a volume is called as a representative elementary volume (REV) (see Figure 2). In our multi-scale methodology, we further require an REV to be a repeated pattern over a portion of the porous media.

The porosity, ε, is defined as the volume fraction of fluid phase in a porous media.

$$\varepsilon = \frac{\mathrm{V}_f}{\mathrm{V}} \tag{1}$$

Note that the porosity might be defined locally or globally depending on the scale that the volume fraction is calculated. In this study, however, we will assume that the porosity is uniform over the porous media.

B. Darcy Equation and Ergun Correction

As the first attempt to describe the flow of fluid through porous structures, Darcy[1] experimented with gravity driven flow of water through a porous medium of loosely packed, uniform sized particles. He arrived at the following relation for pressure drop and the flow speed:

$$-\nabla p = \frac{\mu}{K} u_D \tag{2}$$

The permeability, K with the units of *length*^{2}, is a measure of fluid flow conductivity of the porous media. The filter velocity, u_D, is defined as:

$$u_D = \frac{\dot{m}}{\rho A} \tag{3}$$

A linear relationship represented by Darcy's Law has been shown to apply to a wide range of problems as long as a Reynolds number based on permeability, $\mathrm{Re}_{\sqrt{K}} = \rho u_D \sqrt{K} / \mu$, is roughly less than unity. At higher Reynolds numbers, inertial effects become comparable to Darcian effects. A correction for this flow regime is suggested by Forchheimer[2] and later by Ergun[3]. Since the form presented here is due to Ergun, we attribute this relation to him.

$$-\partial_i p = \frac{\mu}{K} u_{D_i} + \frac{C_E}{K^{1/2}} \rho \left| u_{D_i} \right| u_{D_i} \tag{4}$$

C. Local Volume Averaging

For an arbitrary property ψ defined for the fluid phase, volume averaging can be carried out as follows[12]:

Intrinsic Averaging:

$$< \psi >^f = \frac{1}{\mathrm{V}_f} \int_{\mathrm{V}_f} \psi \mathrm{dV} \tag{5}$$

Superficial Averaging:

$$< \psi >= \frac{1}{\mathrm{V}} \int_{\mathrm{V}_f} \psi \mathrm{dV} = \varepsilon < \psi >^f \tag{6}$$

In the course of volume averaging the governing equations, we need to replace the average of a gradient (or divergence) with the gradient (or divergence) of an averaged quantity. Slattery[4] used the Reynolds transport theorem and the divergence theorem to arrive at the necessary transformation as shown below:

$$\int_{\mathrm{V_f}} \partial_i \psi \mathrm{dV} = \partial_i \int_{\mathrm{V_f}} \psi \mathrm{dV} + \int_{\mathrm{A_{sf}}} \psi n_i \mathrm{dA} \tag{7}$$

Or

$$< \partial_i \psi >= \partial_i < \psi > + \frac{1}{\mathrm{V}} \int_{\mathrm{A_{sf}}} \psi n_i \mathrm{dA} \tag{8}$$

$$< \partial_i \psi_i >^f = \partial_i < \psi_i >^f + \frac{1}{\mathrm{V}_f} \int_{\mathrm{A_{sf}}} \psi_i n_i \mathrm{dA} \tag{9}$$

$$< \partial_i \psi_i >= \varepsilon < \partial_i \psi_i >^f \tag{10}$$

In the local volume averaging procedure discussed below, we consider that the flow is incompressible with constant viscosity. We further consider that the porosity is constant throughout the porous media. These aspects can be generalized.

1. *Averaging of the Continuity Equation*

The continuity equation can be written as

$$\frac{\partial \rho}{\partial t} + \partial_i(\rho u_i) = 0 \tag{11}$$

When volume averaged, Eq. (11) becomes:

$$\frac{\partial < \rho >}{\partial t} + < \partial_i(\rho u_i) > = \frac{\partial < \rho >}{\partial t} + \partial_i < \rho u_i > + \frac{1}{\mathrm{V}} \int_{\mathrm{A}_{sf}} \rho u_i n_i \mathrm{dA} = 0 \tag{12}$$

Since the fluid will be at rest at the solid-fluid interface due to the no-slip condition, the last term in Eq. (12) vanishes, and we get:

$$\frac{\partial < \rho >}{\partial t} + \partial_i < \rho u_i > = 0 \tag{13}$$

Thus, the continuity equation is unchanged by local volume averaging for incompressible flow. In the case of compressible flow, we need to have a special treatment for averaging of the product of the density and the velocity component.

2. *Averaging of the Momentum Equation*

Averaging of the momentum equation for incompressible flows with no body forces yields the following equation:

$$\rho \frac{\partial < u_i >}{\partial t} + \rho < \partial_j u_i u_j > = < \partial_j \mathrm{T}_{ij} > \tag{14}$$

For a Newtonian fluid, the stress tensor is:

$$\mathrm{T}_{ij} = -p\delta_{ij} + 2\mu\, \mathrm{S}_{ij} \tag{15}$$

where $\mathrm{S}_{ij} = \frac{1}{2}\left(\partial_i u_j + \partial_j u_i\right)$, thus for an incompressible flow with constant viscosity

$$\partial_j \mathrm{T}_{ij} = -\partial_i p + \mu\, \partial_j^2 u_i \tag{16}$$

Volume averaging of Eq. (16) yields:

$$\begin{aligned} < \partial_j \mathrm{T}_{ij} > &= \partial_j < \mathrm{T}_{ij} > + \frac{1}{\mathrm{V}} \int_{\mathrm{A}_{sf}} \mathrm{T}_{ij} n_j \mathrm{dA} \\ &= -\partial_i < p > + 2\mu\, \partial_j < \mathrm{S}_{ij} > + \frac{1}{\mathrm{V}} \int_{\mathrm{A}_{sf}} \mathrm{T}_{ij} n_j \mathrm{dA} \end{aligned} \tag{17}$$

where

$$\begin{aligned}\partial_j \langle S_{ij} \rangle &= \frac{1}{2}\partial_j \langle \partial_i u_j + \partial_j u_i \rangle \\ &= \frac{1}{2}\partial_j \left(\partial_i \langle u_j \rangle + \partial_j \langle u_i \rangle + \frac{1}{V}\int_{A_{sf}} \left(u_i n_j + u_j n_i \right) dA \right)\end{aligned} \tag{18}$$

The integral term in Eq. (18) vanishes due to the no-slip condition at the solid-fluid interface. Thus Eq. (14) becomes:

$$\rho \frac{\partial \langle u_i \rangle}{\partial t} + \rho \langle \partial_j u_i u_j \rangle = -\partial_i \langle p \rangle + \mu \partial_j^2 \langle u_i \rangle + \frac{1}{V}\int_{A_{sf}} T_{ij} n_j dA \tag{19}$$

The integral term in Eq. (19) filters the force information at the solid-fluid interface and imposes the integral effect in the volume averaged momentum equation. Note that the convective term still needs to be transformed to a form involving the convection of the volume averaged momentum component. Following the approach of Gray[6], we decompose the velocity as:

$$u_i = \langle u_i \rangle^f + u_i' \tag{20}$$

where $(\,)'$ represents local deviation from intrinsic averaged values. Applying Eq. (20) to the volume-averaged convective term:

$$\begin{aligned}\langle \partial_j u_i u_j \rangle &= \langle \partial_j (\langle u_i \rangle^f + u_i')(\langle u_j \rangle^f + u_j') \rangle \\ &= \langle (\partial_j \langle u_i \rangle^f \langle u_j \rangle^f + \partial_j u_i' u_j' + \partial_j \langle u_i \rangle^f u_j' + \partial_j u_i' \langle u_j \rangle^f) \rangle\end{aligned} \tag{21}$$

One notes that

$$\langle \langle \psi \rangle^f \rangle = \varepsilon \langle \psi \rangle^f \tag{22}$$

$$\langle \psi' \rangle = 0 \tag{23}$$

Thus, Equation (21) simplifies to:

$$\begin{aligned}\langle \partial_j u_i u_j \rangle &= \varepsilon \partial_j \langle u_i \rangle^f \langle u_j \rangle^f + \langle \partial_j u_i' u_j' \rangle \\ &= \frac{1}{\varepsilon}\partial_j \langle u_i \rangle \langle u_j \rangle + \langle \partial_j u_i' u_j' \rangle\end{aligned} \tag{24}$$

Using Eqs. (10) and (24), Eq. (19) becomes:

$$\frac{\rho}{\varepsilon}\frac{\partial \langle u_i \rangle}{\partial t} + \frac{\rho}{\varepsilon^2}\partial_j \langle u_i \rangle \langle u_j \rangle = -\partial_i \langle p \rangle^f + \frac{\mu}{\varepsilon}\partial_j^2 \langle u_i \rangle + \frac{1}{V_f}\int_{A_{sf}} T_{ij} n_j dA - \frac{\rho}{\varepsilon}\langle \partial_j u_i' u_j' \rangle \tag{25}$$

The last two terms on the right hand side of Eq. (25) are surface and volume filter terms, respectively. These terms are related to the interaction of fluid and solid phases and local deviations from averaged values. These terms can not readily be calculated with the global scale (volume averaged) information of flow. This constitutes a closure problem.

3. Averaging of the Energy Equation

Consider the fluid phase energy equation with constant specific heat and no heat sources:

$$(\rho c_p)_f \left(\frac{\partial T_f}{\partial t} + \partial_i u_i T_f \right) = \partial_j k_f \partial_j T_f \tag{26}$$

Applying local volume averaging:

$$(\rho c_p)_f \left(\frac{\partial < T_f >}{\partial t} + < \partial_i u_i T_f > \right) = k_f \, < \partial_j \partial_j T_f > \tag{27}$$

Using Eq. (9), the diffusive term can be expanded as:

$$\begin{aligned} k_f < \partial_j \partial_j T_f > &= k_f \partial_j < \partial_j T_f > + \frac{k_f}{\mathrm{V}} \int_{\mathrm{A}_{sf}} n_j \partial_j T_f \, \mathrm{dA} \\ &= k_f \partial_j \partial_j < T_f > + \frac{k_f}{\mathrm{V}} \partial_j \int_{\mathrm{A}_{sf}} n_j T_f \, \mathrm{dA} + \frac{k_f}{\mathrm{V}} \int_{\mathrm{A}_{sf}} n_j \partial_j T_f \, \mathrm{dA} \end{aligned} \tag{28}$$

Defining a local temperature deviation as:

$$T_f = < T_f >^f + T_f' \tag{29}$$

and employing the divergence theorem and Eq. (29), the second integral term in Eq. (28) becomes:

$$\int_{\mathrm{A}_{sf}} n_j T_f \, \mathrm{dA} = \int_{\mathrm{A}_{sf}} n_j < T_f >^{\mathrm{f}} \mathrm{dA} + \int_{\mathrm{A}_{sf}} n_j T_f' \, \mathrm{dA} = \int_{\mathrm{V}} \partial_j < T_f >^{\mathrm{f}} \mathrm{dV} + \int_{\mathrm{A}_{sf}} n_j T_f' \, \mathrm{dA} \tag{30}$$

Noting that the variation of an averaged quantity within the averaging volume itself is zero,

$$\int_{\mathrm{V}} \partial_j < T_f >^{\mathrm{f}} \mathrm{dV} = 0 \tag{31}$$

we arrive at the averaged diffusion term:

$$k_f < \partial_j \partial_j T_f > = k_f \partial_j \partial_j < T_f > + \frac{k_f}{\mathrm{V}} \partial_j \int_{\mathrm{A}_{sf}} n_j T_f' \, \mathrm{dA} + \frac{k_f}{\mathrm{V}} \int_{\mathrm{A}_{sf}} n_j \partial_j T_f \, \mathrm{dA} \tag{32}$$

Averaging of the convection term yields:

$$< \partial_i u_i T_f > = \partial_i < u_i T_f > + \frac{1}{\mathrm{V}} \int_{\mathrm{A}_{sf}} u_i T_f n_i \, \mathrm{dA} \tag{33}$$

The integral term on the right hand side of Eq. (33) vanishes due to no-slip condition at the solid-fluid walls. Using Eqs. (20) and (29), we decompose the convective term as:

$$\begin{aligned} < \partial_i u_i T_f > &= \partial_i < u_i T_f > = \partial_i < (< u_i >^f + u_i')(< T_f >^f + T_f') > \\ &= \partial_i << u_i >^f < T_f >^f + < u_i >^f T_f' + u_i' < T_f >^f + u_i' T_f' > \\ &= \varepsilon \partial_i < u_i >^f < T_f >^f + \varepsilon \partial_i < u_i >^f < T_f' >^f + \varepsilon \partial_i < u_i' >^f < T_f >^f + \varepsilon \partial_i < u_i' T_f' >^f \end{aligned} \tag{34}$$

Knowing that $< \psi' > = 0$, the volume-averaged convection term is obtained:

$$< \partial_i u_i T_f >= \varepsilon \partial_i < u_i >^f < T_f >^f + \varepsilon \partial_i < u_i' T_f' >^f \tag{35}$$

Substituting Eq. (32) and Eq. (35) in Eq. (27), we obtain the volume-averaged energy equation for the fluid phase:

$$\varepsilon(\rho c_p)_f \left(\frac{\partial < T_f >^f}{\partial t} + \partial_i < u_i >^f < T_f >^f + \partial_i < u_i' T_f' >^f \right) = \varepsilon k_f \partial_j \partial_j < T_f >^f + \frac{k_f}{\mathrm{V}} \partial_j \int_{\mathrm{A}_{sf}} n_j T_f' \mathrm{dA} + \frac{k_f}{\mathrm{V}} \int_{\mathrm{A}_{sf}} n_j \partial_j T_f \mathrm{dA} \tag{36}$$

Similarly, in the solid phase, the volume-averaged energy equation is:

$$(1-\varepsilon)(\rho c_p)_s \frac{\partial < T_s >^s}{\partial t} = (1-\varepsilon) k_s \partial_j \partial_j < T_s >^s + \frac{k_s}{\mathrm{V}} \partial_j \int_{\mathrm{A}_{fs}} n_j T_s' \mathrm{dA} + \frac{k_s}{\mathrm{V}} \int_{\mathrm{A}_{fs}} n_j \partial_j T_s \mathrm{dA} \tag{37}$$

In many practical problems, the temperature difference between the solid and fluid phases inside a REV is much smaller than the global scale temperature variation. This condition is met if the REV is much smaller compared to global length scale, there is no heat generation or loss inside the REV and temperature distribution does not vary or vary slowly over time. Under these conditions, we can assume "local thermodynamic equilibrium" (LTE) which grants:

$$< T_f >^f = < T_s >^s = < T > \tag{38}$$

At the solid-fluid interface, the following boundary conditions apply:

$$T_f' \big|_{\mathrm{A}_{sf}} = T_s' \big|_{\mathrm{A}_{sf}} \tag{39}$$

$$k_f \partial_j T_f \big|_{\mathrm{A}_{sf}} = k_s \partial_j T_s \big|_{\mathrm{A}_{sf}} \tag{40}$$

Also noting that $\mathbf{n}_{sf} = -\mathbf{n}_{fs}$, and adding Eqs. (36) and (37), we obtain the local volume averaged energy equation:

$$\begin{aligned} [\varepsilon(\rho c_p)_f + (1-\varepsilon)(\rho c_p)_s] \frac{\partial < T >}{\partial t} + (\rho c_p)_f \partial_i < u_i >< T > \; &= \; [\varepsilon k_f + (1-\varepsilon) k_s] \partial_j \partial_j < T > + \frac{k_f - k_s}{\mathrm{V}} \partial_j \int_{\mathrm{A}_{sf}} n_j T_f' \mathrm{dA} \\ &- \; \varepsilon(\rho c_p)_f \partial_i < u_i' T_f' >^f \end{aligned} \tag{41}$$

D. Closure Terms

The closure problem in porous media is often handled by heuristically replacing the closure terms in Eq. (25) by Darcy and Ergun terms given in Eq. (4).

$$\frac{\rho}{\varepsilon} \frac{\partial < u_i >}{\partial t} + \frac{\rho}{\varepsilon^2} \partial_j < u_i >< u_j > = -\partial_i < p >^f + \frac{\mu}{\varepsilon} \partial_j^2 < u_i > - \frac{\mu}{K} < u_i > - \frac{C_E}{K^{1/2}} \rho \big| < u_i > \big| < u_i > \tag{42}$$

While Eq. (4) only relates the bulk pressure drop to the total mass flow rate, the solution of Eq. (42) provides locally-averaged flow field information throughout the porous media. Eq. (42) is very similar in form to the Navier-Stokes equations. This enables us to easily handle both conjugate open flow (without porous media) and porous flow problems and permits application of no-slip conditions at the solid walls bounding the solid matrix. By this treatment, the problem is reduced to the determination of two parameters, namely, permeability, K and Ergun coefficient, C_E. These parameters are either estimated through existing empirical correlations or found via

experimentation for specific types of porous media. Note that there is no fundamental reason for Eq. (42) to be correct. However, in many tightly packed porous media, momentum loss is mostly due to the pore scale flow structures which are represented by the two closure terms in Eq. (25). Thus, generally, Eq. (42) is expected to closely follow Eq. (4).

Following the conventional closure approach of the energy equation, invoking local thermal equilibrium assumption, we first introduce the constitutive relation suggested by Nozad et al.[9] :

$$T' = \mathrm{b}_i \partial_i < T >^f \tag{43}$$

where b_i is a space dependent vector transformation function. Also using the definition of the dispersion tensor:

$$\mathrm{D}_{ij}^d = - < u_i' \mathrm{b}_j > \tag{44}$$

The local volume-averaged energy equation (Eq. (41)) can be transformed to:

$$[\varepsilon(\rho c_p)_f + (1-\varepsilon)(\rho c_p)_s] \frac{\partial < T >}{\partial t} + (\rho c_p)_f \partial_i < u_i >< T >= (\rho c_p)_f \partial_i (\mathrm{D}_{ij}) \partial_j < T > \tag{45}$$

where D_{ij} is the total effective thermal diffusivity tensor given as:

$$\mathrm{D}_{ij} = \frac{\mathrm{K}_{ij}^e}{(\rho c_p)_f} + \varepsilon \mathrm{D}_{ij}^d \tag{46}$$

Here K_{ij}^e is the effective thermal conductivity tensor. A detailed account for development of Eq. (45) can be found in Ref. 11. Our purpose here is to demonstrate that Eq. (41) can be transformed to a form similar to the regular point energy equation. However, in our current work, there is no need to adopt this approach.

Conventional approaches to the closure problem in volume-averaged momentum and energy equations involve heuristic assumptions, constitutive relations and empirical dependence. This disturbs practicality of numerical simulations. Instead, we attempt to compute the closure terms directly over typical pore geometries observed in porous media. Basically, we then have two levels of numerical simulations; pore scale flow simulations conducted over typical pore models, and global scale flow simulations facilitating the closure terms supplied by pore scale simulations. This helps us avoid making any further simplifications other than the assumptions undertaken during the derivation of the volume averaged governing equations. More importantly, this strategy provides a stand alone method which can be applied completely free of empiricism. Computational cost associated with this multi-scale approach strongly depends on the level of uniformity and complexity of the pores. For a uniform porous media, only one pore model is needed.

With the multi-scale approach, we can either evaluate the closure terms in Eq. (25) directly or deduce the permeability and Ergun coefficients of the porous media by matching Eqs. (25) and (42):

$$K = -\mu < u_i > \left[\frac{1}{\mathrm{V}_f} \int_{\mathrm{A}_{sf}} \mathrm{T}_{ij} n_j \mathrm{dA} \right]^{-1} \tag{47}$$

$$C_E = \frac{K^{1/2}}{|< u_i >| < u_i >} \partial_j < u_i' u_j' >^f \tag{48}$$

The direct closure method is more desirable since it avoids the heuristic assumption of replacing the closure terms with the Ergun relation. However, we use the latter in the test case presented here in order to compare our results to Tully et al.[15] and investigate the behavior of the permeability and Ergun coefficients with changing flow speed. The flow chart of the present multi-scale algorithm, for both approaches, is presented in Figure 3.

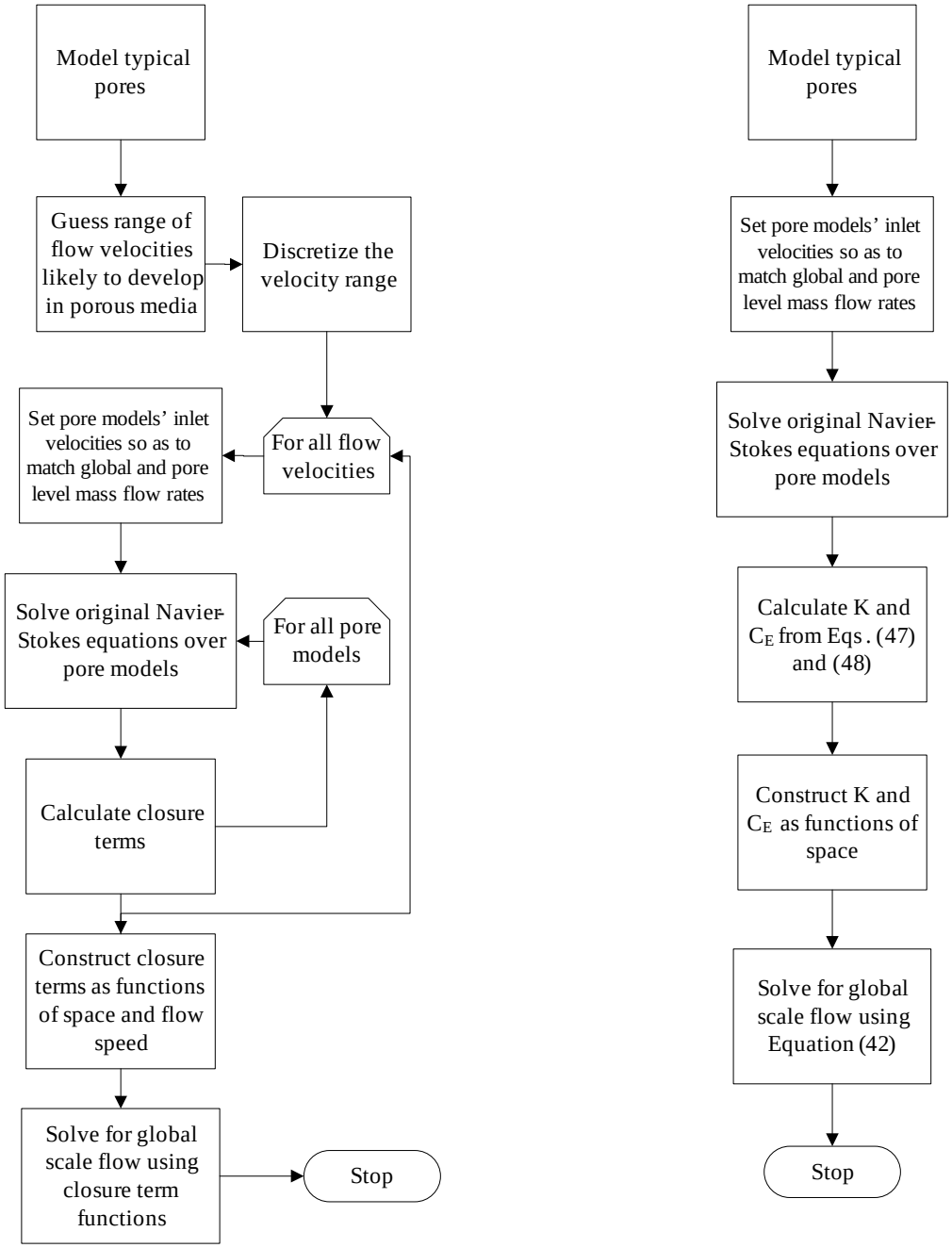

Figure 3. The multi-scale algorithm flowcharts for direct closure computations (left), and closure estimates via permeability and Ergun coefficients (right).

E. Numerical Method

We have shown that for the flow through porous media, the continuity equation is unchanged and momentum equation is very similar in form to the regular Navier-Stokes equations with additional momentum source terms and the other terms modified by factors of porosity, ε. Thus a Navier-Stokes solver can easily be modified to account for porous media.

We utilize a pressure-based finite volume solver (Ref. 14) for multi-block body-fitted grids which enables us to solve for combined open and porous domains. Standard central difference operator is used for pressure and

diffusive fluxes whereas a second order upwind method is used for convective fluxes. Using a short-hand notation for the u-momentum equation with collocated arrangement of variables, the discretized equation can be written as

$$A_p u_p = \sum A_{nbr} u_{nbr} + S \tag{49}$$

where *nbr* represents the six neighboring points (East, West, North, South, Top and Bottom) of the node *p*. A_{nbr} represents the corresponding contributions. *S* term accounts for the sources that cannot be expressed in terms of the point *p* and its immediate neighbors. It includes contributions from the pressure term, cross-derivative diffusion terms and higher-order contribution of the convective fluxes. In porous regions, another source term S_{porous} is added to reflect the effect of momentum loss experienced.

$$A_p u_p = \sum A_{nbr} u_{nbr} + S + S_{porous} \tag{50}$$

Also A_p and A_{nbr} are modified to account for the porosity factors as shown in Eq. (25).

The extended SIMPLEC (Consistent SIMPLE) (Ref. 7-8) algorithm is employed. Specifically, we employ combined Cartesian and contravariant velocity components, cast in a finite volume form of the governing equations, for the primary velocity variable and flux computations, respectively (Ref. 10).

III. Results and Discussions

A. Isothermal Non-Darcian Flow through a Drilled Orifice Plate

This test case is designed for validating our multi-scale methodology in a problem with uniform and well defined pore geometry. The porous material used herein is a metallic plate with an array of uniform and evenly distributed drilled holes. The hole pattern detail is depicted in Figure 4. The porous plate is inserted in a cylindrical channel test section. This problem was studied before by Tully et al.[15] both numerically and experimentally. Experimental and computational domains used in their study are presented in Figure 5. Computations are performed over a simplified domain to avoid excessive cost. However, the simplification undertaken may be questioned on the grounds that the velocity profile entering the porous plate in the experimental case is likely to be more complicated than what is realized in the computational domain. We address this question later on by studying the sensitivity of the numerically obtained pressure drop to the inlet velocity profile shape. First we try to reproduce the results previously reported by Tully et al.[15]

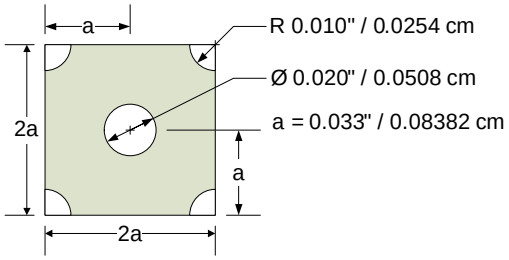

The porosity of the drilled plate can easily be calculated as:

$$\varepsilon = \frac{\text{Void Volume}}{\text{Total Volume}} = \frac{2\pi\left(\frac{\phi}{2}\right)^2}{(2a)^2} = 0.1442 \tag{51}$$

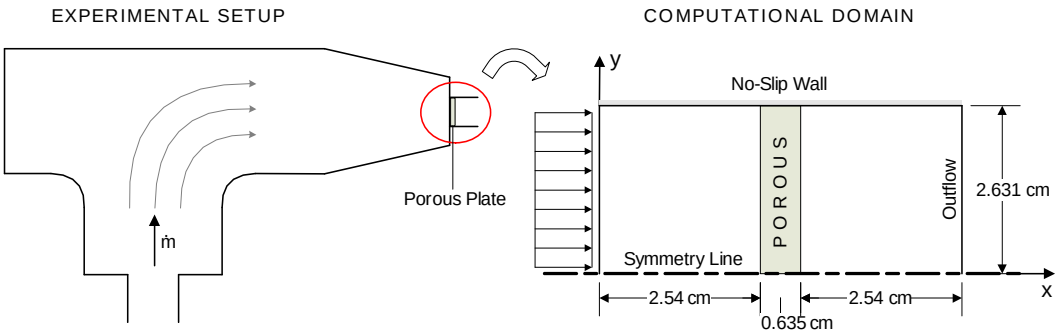

Figure 5. Experimental setup and computational domain.

Input parameters corresponding to experimental data points are summarized in Table 1. Tully et al.[15] estimates the permeability and Ergun coefficient of the porous material by investigating the experimental pressure drop (across the plate at the centerline) vs. filter velocity data. Coefficients of a quadratic curve fit to this data can be used to calculate the K and C_E values for best fit to experimental data. The parameters they derived for this case are

$$\begin{aligned} K &= 5.740E-9 \text{ m}^2 \\ C_E &= 0.487 \end{aligned} \tag{52}$$

Table 1. Summary of experimental conditions.

Fluid properties (Air @ 24.2 °C)			Inlet Filter Velocities (m/s)	
Density (ρ)	1.1875	kg/m^3	U_{D1}	10.5
Dynamic Viscosity (μ)	1.8048E-5	kg/m.s	U_{D2}	13.1
Specific Heat (c_P)	1006.2	J/kg.K	U_{D3}	16.3
Thermal Conductivity (k)	0.025913	W/m.K	U_{D4}	18.1
			U_{D5}	20.1
			U_{D6}	23.3
			U_{D7}	25.8

1. Empirically deduced porous media model parameters (from Tully et al.[15])

First, we present global scale computational results using permeability and Ergun coefficient values provided by Tully et al.[15] Figure 6 shows that the computational and experimental values of the pressure drop agree well with each other. This is an expected behavior since permeability and Ergun coefficient were empirically determined to grant the best fit to the experimental data. We include this approach to help establish a baseline model to help contrast this and our multi-scale approach.

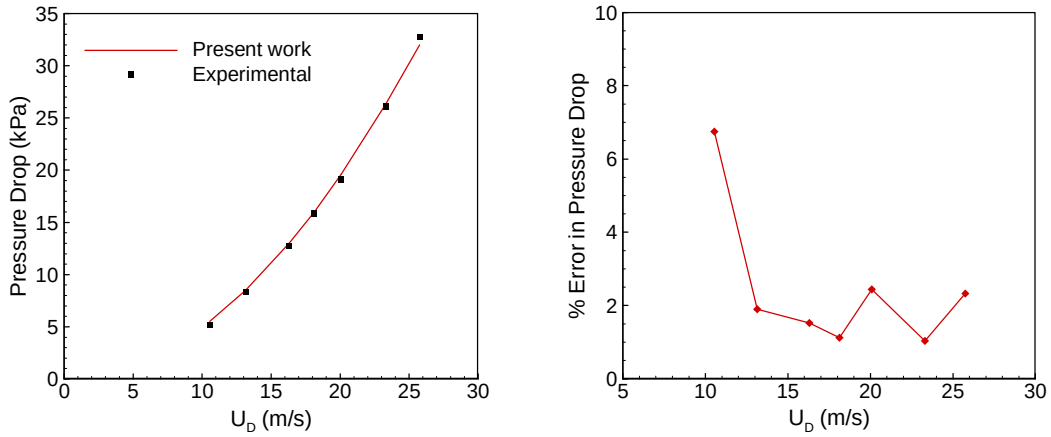

Figure 6. Measured and computed pressure drop results across the porous plate along the centerline and percentage error relative to experimental data provided by Tully et al.[15]

2. Multi-Scale Model

Here, we apply the described multi-scale methodology to simulate the same problem independent of experimental results. For closure, we will use the momentum equation in the form of Eq. (42) where we evaluate the permeability and the Ergun coefficients via Eqs. (47) and (48). We prefer this form here in order to be able to compare our results with Tully et al.[15] and assess the variance of these parameters with the flow speed.

Note that the drilled plate pore geometry is uniform, i.e., a single representative elementary volume (REV) is sufficient to describe the porous medium. An REV for the drilled plate can be chosen as shown in Figure 7.

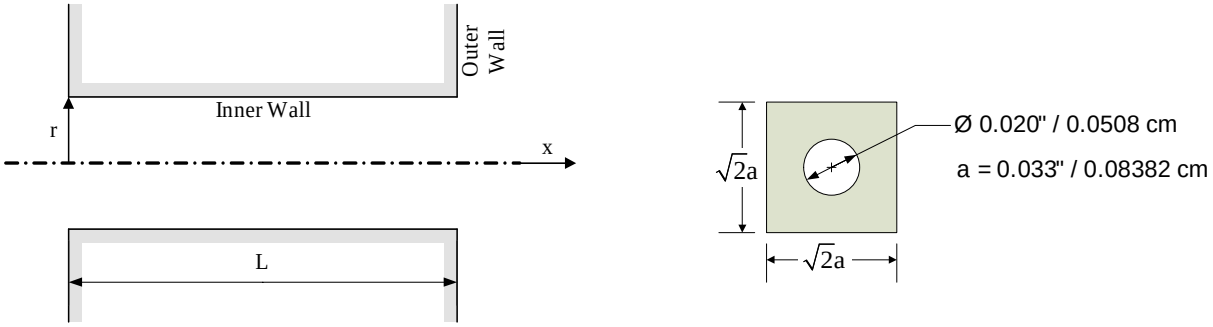

Figure 7. Representative elementary volume (REV).

We could have chosen only a small section of the tube as an REV since it would be a repeating pattern. However, by extending the REV to full length of the tube, we include the averaged effect of the developing flow region. Numerical model of this domain is shown in Figure 8. An axisymmetric domain is used for the computations. In order to conserve mass flux, the inlet velocity for this domain will be $1/\varepsilon$ times higher than the inlet velocity of the global domain where $\varepsilon = 0.1442$ is the porosity.

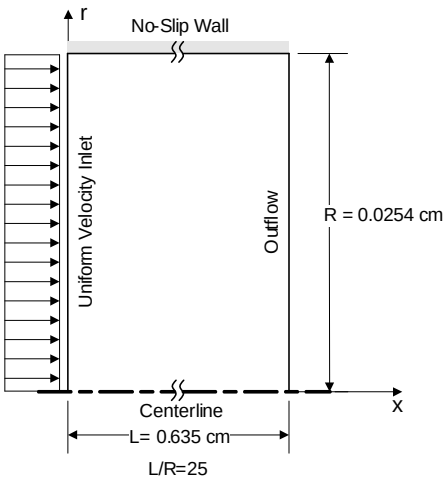

Figure 8. Numerical domain for pore scale analysis.

Permeability

In this section, we estimate the permeability of the drilled plate using Eq. (47). Note that this equation simplifies the problem in hand greatly. Thus far, we have treated the drilled plate as an isotropic porous media although it is clearly not isotropic. However, the flow through the plate is essentially axial (perpendicular to plate). Thus we are only interested in the axial component of the flow for this particular case and we can express Eq. (47) as:

$$K = -\mu < u_i > \mathrm{V}_f \left[\int_{\mathrm{A}_{inner\ wall}} \mu \left(\frac{\partial u_x}{\partial r} + \frac{\partial u_r}{\partial x} \right) \mathrm{dA}_r \right]^{-1} \tag{53}$$

Note that the outer wall is not a part of the repeating pattern and the effect of pressure distribution on the outer wall will appear as an acceleration of the flow inside the tube to conserve total mass flux rate through the plate. On the other hand, pressure distribution on the inner wall does not appear in Eq. (53) because $p\delta_{xr}n_r = 0$.

Also from Figure 7, we immediately see that:

$$\left.\frac{\partial u_x}{\partial x}\right|_{outer\ wall} = \left.\frac{\partial u_r}{\partial x}\right|_{inner\ wall} = 0 \tag{54}$$

Thus, Eq. (53) reduces to

$$K = -\mu < u_i > \mathrm{V}_f \left[\int_{\mathrm{A}_{inner\ wall}} \mu \frac{\partial u_x}{\partial r} \mathrm{dA}_r \right]^{-1} \tag{55}$$

The integral term is the net skin friction force applied on the inner wall of the tube. Denoting this by F_τ, we get:

$$K = -\frac{\mu < u_i > \mathrm{V}_f}{F_\tau} = -\frac{\mu < u_i > (\pi r^2 L)}{F_\tau} \tag{56}$$

F_τ can easily be calculated by numerical integration.

Ergun Coefficient

For permeability, we only used the stress information on the solid-fluid boundary of the pore. On the other hand, the Ergun term involves the inertial effects in the fluid volume passing through the pores. Remember the expression derived for the Ergun term

$$C_E = \frac{K^{1/2}}{|<u_i>|<u_i>} \partial_j <u_i' u_j'>^f \tag{57}$$

For a 2-D axial flow, the volume averaged term can be approximated as

$$\partial_j <u_i' u_j'>^f \approx \frac{1}{V_f} \sum_{n=1}^{ncell} \left[\frac{\partial}{\partial x} u_x^2 + \frac{\partial}{\partial r}(u_x u_r) \right] \tag{58}$$

where the derivative expressions are evaluated with second order central finite differences.

3. Model Assessment

For the flow speeds corresponding to the global scale cases listed in Table 1, we have estimated the permeability and Ergun coefficients by employing the methods summarized above. Using these parameters, we have performed the global scale computations and compared our results to the experimental pressure drop data. Results are given in Table 2 and Figure 9 with the following conventions:

ΔP_E : Experimental measurement of pressure drop across the plate

ΔP_C : Computed pressure drop across the plate with K and C_E estimated from pore scale analysis

$\frac{\Delta P_{C_E}}{\Delta P_K}$: Proportion of pressure drops due to inertial and Darcian terms

Table 2. Pore level analysis results for drilled plate

Case	U_D (m/s)	U_D/ε	Re_d	$\mathrm{Re}_{\sqrt{K}}$	K	C_E	ΔP_C (Pa)	ΔP_E (Pa)	$\Delta P_{C_E}/\Delta P_K$
1	10.5	72.82	2434	43	3.89×10^{-9}	0.380	5263	5159	16.4
2	13.1	90.85	3033	52	3.63×10^{-9}	0.372	8227	8331	19.3
3	16.3	113.0	3772	62	3.38×10^{-9}	0.364	12818	12790	22.6
4	18.1	125.5	4195	68	3.26×10^{-9}	0.359	15823	15830	24.4
5	20.1	139.4	4653	74	3.14×10^{-9}	0.355	19603	19140	26.3
6	23.3	161.6	5400	84	2.98×10^{-9}	0.349	26481	26070	29.2
7	25.8	178.9	5970	91	2.88×10^{-9}	0.344	32487	32750	31.3

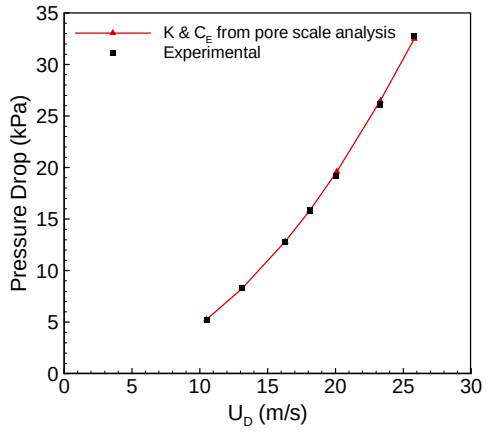

Figure 9. Pressure drop results in comparison to experimental data by Tully et al.[15]

We have mentioned earlier that the inertial effects in the flow become pronounced for $Re_{\sqrt{K}} > 1$. Table 2 shows that for the whole range of available experimental data, the inertial term in the porous region is dominant. And thus

almost the entire pressure drop is imposed by this term. Denoting the additional pressure drop due to the existence of the porous material by P_Q, we have

$$P_Q = \frac{\mu}{K} < u_i > + \rho \frac{C_E}{\sqrt{K}} | < u_i > | < u_i > \approx \rho \frac{C_E}{\sqrt{K}} | < u_i > | < u_i > \tag{59}$$

Thus for inertial dominant regime of the flow, we may argue that the only significant parameter in describing the effect of momentum loss in the porous media is $C_E / \sqrt{K}$ which is then analogous to a form of drag coefficient. Furthermore, it is shown in Table 4 that this parameter weakly depends on the flow speed. To test how sensitive the results are to the changes in this parameter, we compare our results for multi-scale method to the ones obtained with fixed values of K and C_E as suggested by Tully et al.[15] Table 3 shows the relative differences. Filter velocity vs. pressure drop curves are presented in Figure 10.

Table 3. Comparison of fixed parameters approach and multi-scale results.

Case	$C_E / \sqrt{K}$	Fixed K and C_E	% Difference in $C_E / \sqrt{K}$	% Difference in ΔP
1	6093	Suggested values	5.2	4.6
2	6174	By Tully et al[8]	4.0	3.2
3	6261	$K = 5.74 \times 10^{-9}$	2.6	1.3
4	6288	$C_E = 0.487$	2.2	1.2
5	6335	$C_E / \sqrt{K} = 6428$	1.4	0.02
6	6393		0.5	0.5
7	6410		0.3	1.5

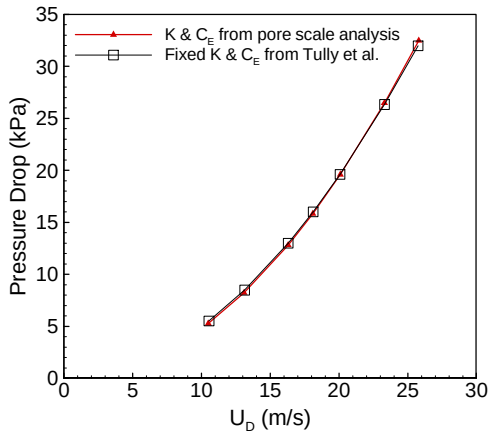

Figure 10. Pressure drop curves for fixed parameters approach vs. multi-scale method.

We observe that the error associated with using fixed values of K and C_E is not significant for inertial dominated flow regime. However, for the slower flow rates, the Darcian term becomes important and the pressure drop is then governed by both K and C_E separately which were shown to be varying with flow speed. Nevertheless, for the current problem, the computed pressure drop doesn't exhibit significant sensitivity to the detailed porous media model parameter values.

4. Assessment of Sensitivity to Skewness of Inlet Profile

In the computations, a parabolic or nearly parabolic velocity profile which is also symmetric across the centerline of the channel exists at the upstream face of the porous plate. However, in the experimental case, a more complex profile is likely to develop due to the turning and contraction of the flow

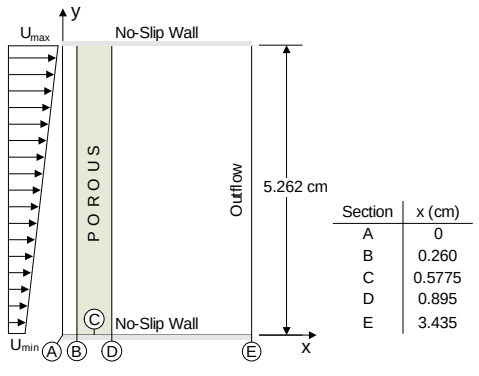

Figure 11. Modified computational domain.

as shown in Figure 5. In this section, sensitivity of pressure drop across the porous plate to non-uniformity of the inlet velocity profile will be tested by comparing results for uniform and skewed velocity profile at the inlet. The entrance section of the computational grid is shortened in order to prevent smearing of the skewed profile before reaching the porous region. The modified computational domain for this analysis is illustrated in Figure 11. Two types of inlet velocity profiles are imposed while keeping the mass flow rate constant:

Uniform with U=23.31 m/s
Trapezoidal with U_{min}=11.65 m/s and U_{max}=34.96 m/s

Figure 12 shows the change in velocity profiles across the porous plate. We see that the two velocity profiles tend to get closer towards downstream.

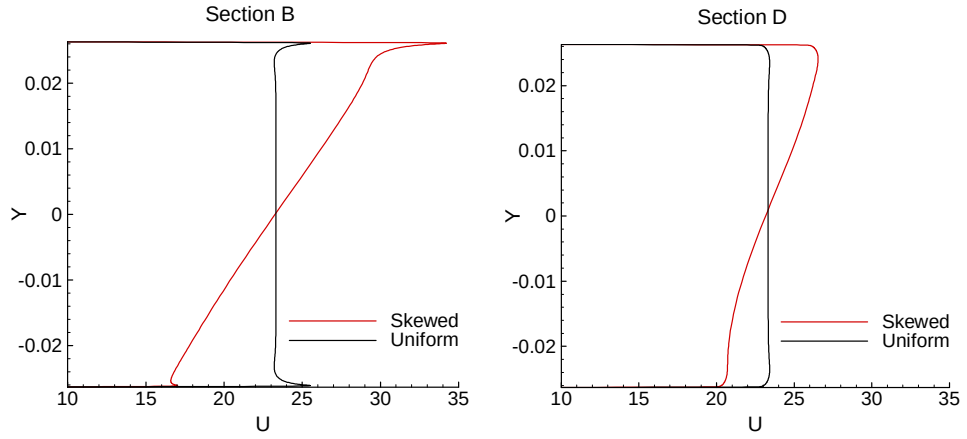

Figure 12. Change in velocity profiles in the porous section.

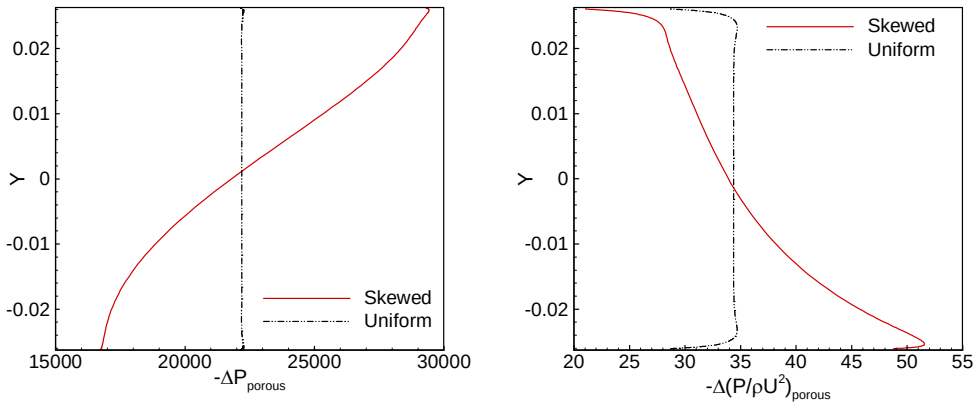

Figure 13. Profiles of pressure drop (left) and mass normalized pressure drop (right) across the porous plate.

Figure 13 shows pressure drop profiles across the porous region. While the pressure drop is almost constant across the whole channel height for the uniform inlet case, skewed profile case shows +32% to -27% variation with respect to the uniform inlet case. More insight to the comparison can be provided by examining the pressure drop normalized with local convective scale. Average values of the pressure drops are provided in Table 4. We observe that the difference caused by the skewness of the inlet velocity profile is not trivial. However, we may argue that the fully skewed inlet profile as tested is an extreme case.

Table 4. Summary of average pressure drops across the porous plate.

	Skewed Inlet Velocity Profile	Uniform Inlet Velocity Profile	%Difference
$\Delta\bar{P}$	2.285E+4	2.220E+4	2.93
$\Delta\bar{P}^*$	37.04	33.33	11.1

$$\Delta\bar{P} = \frac{1}{ny}\sum_{j=1}^{ny}\Delta P_{porous}$$

$$\Delta\bar{P}^* = \frac{1}{ny}\sum_{j=1}^{ny}\Delta\left(\frac{P}{\rho U^2}\right)_{porous}$$

B. Heat Transfer in a Channel with 90-deg Turning Flow

A heat transfer problem through a 90-deg turning channel filled with porous metallic foam is studied. The problem definition schematic is given in Figure 14. A constant temperature and velocity inlet is considered along a portion W_j of the top wall. A constant heat flux condition is imposed through the bottom wall while other walls are kept adiabatic.

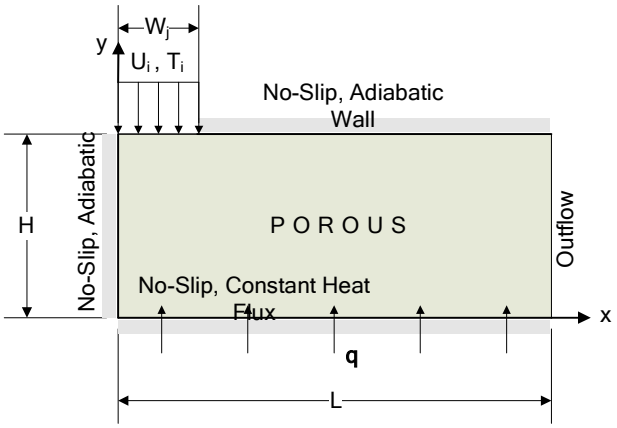

Figure 14. 90-deg turning flow problem description.

Global scale computations are performed using Eqs. (42) and (45) where closure parameters used are given in Table 5.

Table 5. Closure parameters of the metallic foam as reported by Tzeng et al.[16]

Porosity, ε	Permeability, K	Ergun Coefficient, C_E	Effective Thermal Conductivity, K^e
0.93	2.34E-7 (m^2)	0.0476	5.23 (W/m.K)

We investigate the dimensionless temperature distribution along the heated wall and skin friction coefficient across the domain.

$$\theta_w = \frac{T_{wall} - T_{inlet}}{qH / k_{fluid}} \tag{60}$$

$$C_f = \frac{p_i - p_e}{1/2\rho_f U_e^2} \tag{61}$$

The purpose of this test case is to present preliminary computational results involving heat transfer. As shown in Figure 15, the thermal characteristics are more sensitive to the Reynolds number than the skin friction coefficient.

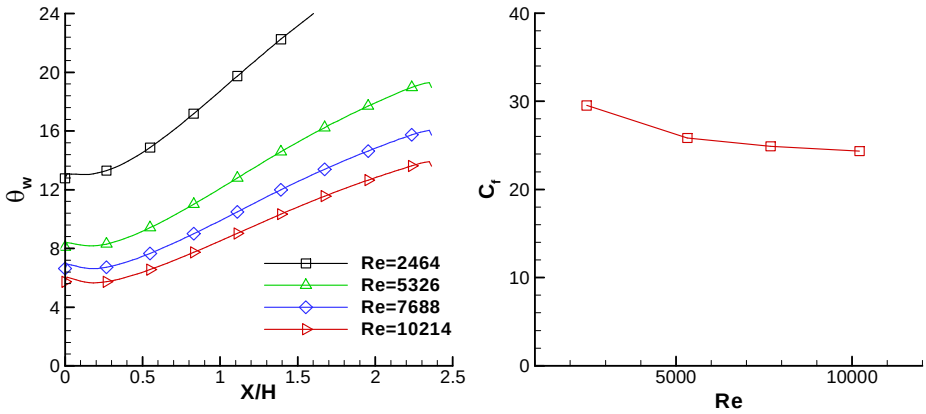

Figure 15. Dimensionless temperature distribution along the bottom heated wall (left) and skin friction coefficient with changing Reynolds number (right).

IV. Summary and Conclusion

We have developed a multi-scale strategy for efficient numerical simulations of flows through porous media. The key feature of this method is independence from empiricism. To assess the present approach and those presented in the literature, we have assessed the permeability and the Ergun coefficient and compared the computed values with those estimated empirically. Furthermore, the performance of the model has been tested. Both the permeability and Ergun coefficient are flow properties; in contrast, the empirical approach typically results in constant values of these parameters independent of the flow conditions. Hence, the present multi-scale approach is more versatile and can account for the possible changes in flow characteristics. Furthermore, Eq. (48) shows that the Ergun coefficient scales with the square root of the permeability. So, a decrease in permeability also yields a decrease in Ergun coefficient. Thus, error in pressure drop due to inaccurate calculation of permeability tends to be compensated by the inertial term through the Ergun coefficient. Furthermore, the sensitivity of the pressure drop to the detailed model parameters is assessed in the context of a test problem.

Rigimesh is formed by pressing layers of steel wire meshes. Thus, a Rigimesh plate is denser towards the faces making porosity smaller. We mentioned before that in the case of SSME, a Rigimesh plate with about 9% void space is used. This implies substantial acceleration of flow inside the pores. Thus, the compressibility effect is likely to become significant. These issues will be address in future efforts.

Acknowledgments

This study is supported by the NASA Constellation University Institute Program (CUIP). We have benefited from collaboration with Professors Bruce Carroll and Jacob Chung of the University of Florida, and Mr. Kevin Tucker of NASA Marshall Space Flight Center.

References

[1]Darcy H., *Les Fontaines Publiques de la ville de Dijon*, Dalmont, Paris, 1856.
[2]Forchheimer P., "Wasserbewegung durch Boden," *Z Ver Deutsch Ing*, 45:1782-1788, 1901.
[3]Ergun S., "Fluid Flow Through Packed Column," *Chem Eng Prog* 48:89-94, 1952.
[4]Slattery J. C., "Single-phase Flow through Porous Media," *AICHE J* 15:866-872, 1969.
[5]Ward J. C., "Turbulent Flow in Porous Media," *J Hyd Div ASCE* 90(HY5):1-12, 1969.
[6]Gray, W.G., "A Derivation of the Equations for Multiphase Transport," Chem. Engng. Sci. 30, 229-233, 1975.
[7] Patankar, S. V., *Numerical Heat Transfer and Fluid Flow*, Hemisphere, Washington, D.C., 1980.
[8] Van Doormaal, J. P. and Raithby, G. D., "Enhancements of the simple method for predicting incompressible fluid flows," *Numerical Heat Transfer*, 7:147–163, 1984.
[9] Nozad, I., Carbonell, R. G., Whitaker, S., "Heat Conduction in Multi-Phase Systems I: Theory and Experiments for Two-Phase Systems," *Chem. Engng. Sci.*, 40, 843-855, 1985.
[10] Shyy, W., *Computational Modeling for Fluid Flow and Interfacial Transport, Elsevier Science Publishers*, Amsterdam, 1994.
[11] Kaviany, M., *Principles of Heat Transfer in Porous Media*, Springer-Verlag, New York, 1995
[12] du Plesis P., *Fluid Transport in Porous Media*, Computational Mechanics Publications, Southampton, 1997.

[13] Martin A., Saltiel C., Shyy W., "Frictional Losses and Convection Heat Transfer in Sparse, Periodic Cylinder Arrays in Cross Flow," *Int J Heat Mass Transfer* 41:2383-2397, 1998.
[14] Thakur, S., Wright, J., and Shyy,W., "Stream: A computational fluid dynamics and heat transfer Navier-Stokes solver. theory and applications," Streamline Numerics, Inc. and Computational Thermo-Fluids Laboratory, Department of Mechanical and Aerospace Engineering Technical Report, Gainesville, Florida, 2002.
[15] Tully L. R., Omar, A., Chung, J. N., and Carroll, B. F., "Fluid flow and heat transfer in a liquid rocket fuel injector," *AIAA/ASME/SAE/ASEE Joint Propulsion Conference & Exhibit*, AIAA-2005-4127, 2005.
[16] Sheng-Chung Tzeng, Tzer-Ming Jeng, "Convective Heat Transfer in Porous Channels with 90-deg Turned Flow," *International Journal of Heat and Mass Transfer*, Vol. 49, pp.1452-1461, 2006.